16. Data Report: Magnetostratigraphy and Biostratigraphy Correlation in Pelagic Sediments, ODP Site 1225, Eastern Equatorial Pacific[1]

Sachiko Niitsuma,[2] Kathryn H. Ford,[3] Masao Iwai,[4]
Shun Chiyonobu,[2] and Tokiyuki Sato[5]

ABSTRACT

Shipboard investigation of magnetostratigraphy and shore-based investigation of diatoms and calcareous nannofossils were used to identify datum events in sedimentary successions collected at Ocean Drilling Program (ODP) Leg 201 Site 1225. The goal was to extend the magnetic record previously studied at the same site, ODP Leg 138 Site 851, and provide a comprehensive age model for Site 1225. Two high–magnetic intensity zones at 0–70 and 200–255 meters below seafloor (mbsf) were correlated with lithologic Subunits IA and IC in Hole 1225A. Subunit IA (0–70 mbsf) contains the magnetic reversal record until the Cochiti Subchronozone (3.8 Ma) and has a sedimentation rate of 1.7 cm/k.y. This agrees with previous work done at Site 851. Subunit IC (200–255 mbsf) was not sampled at Site 851. Diatom and nannofossil biostratigraphy constrained this subunit, and we found it to contain the magnetic reversal record between Subchrons C4n.2r and C5n.2n (8.6–9.7 Ma), yielding a sedimentation rate of 2.7 cm/k.y. Biostratigraphy was used to establish the sedimentation rates within Subunits IB and ID (70–200 mbsf and 255–300 mbsf, respectively). These subunits had higher sedimentation rates (~3.4 cm/k.y.) and coincide with the late Miocene–early Pliocene biogenic bloom event (4.5–7 Ma) and the Miocene global cooling trend (10–15 Ma). High biogenic productivity

[2]Graduate School of Science, Tohoku University, Sendai 980-8578, Japan. Correspondence author:
greigite@ganko.tohoku.ac.jp
[3]Graduate School of Oceanography, University of Rhode Island, South Ferry Road, Narragansett RI 02882, USA.
[4]Department of Natural Environmental Science, Kochi University, Kochi 780-8520, Japan.
[5]Faculty of Engineering and Resource Science, Akita University, Akita 010-0851, Japan.

associated with these subunits resulted in the pyritization of the magnetic signal. In lithologic Subunit ID, basement flow is another factor that may be altering the magnetic signal; however, the good correlation between the biostratigraphy and magnetostratigraphy indicates that the magnetic record was locked-in near the seafloor and suggests the age model is robust.

INTRODUCTION

Site 1225 is located in the eastern equatorial Pacific near the boundary between the South Equatorial Current and the North Equatorial Countercurrent west of the East Pacific Rise (Fig. F1). The site lies in the topographic high created by the rain of biogenic debris from the relatively high productivity equatorial ocean. Site 1225 is adjacent to Ocean Drilling Program (ODP) Leg 138 Site 851. The main features of the sedimentary succession were documented during Leg 138 (Shipboard Scientific Party, 1992; Pisias, Mayer, Janacek, Palmer-Julson, and van Andel, 1995). However, magnetostratigraphy at Site 1225 was not measured or interpreted below 150 meters below seafloor (mbsf) based on the assumption that diagenesis had destroyed the magnetic signal (Shipboard Scientific Party, 1992). More efficient shipboard measurements at Site 1225 illustrated a second zone containing magnetic polarity below 200 mbsf (Shipboard Scientific Party, 2003). The goal of this project is to refine the chronology of this site using both magnetostratigraphic and biostratigraphic techniques.

METHODS

Sampling

For the paleomagnetic and biostratigraphic analyses, samples were collected from Holes 1225A and 1225C. From Hole 1225A, all core catcher samples except those from Cores 201-1225A-28X and 29P were collected. The total volume of each core catcher sample was 50 cm³. This volume was subsampled to 10 cm³ for paleontological analyses. These samples were stored at 4°C until analyzed. From Hole 1225C, 29 discrete 7-cm³ samples were collected for paleomagnetic analysis and stored at room temperature.

Paleomagnetism

A 2G Enterprises superconducting rock magnetometer was used for shipboard pass-through measurements of natural remanent magnetization (NRM) and alternating-field (AF) demagnetization of split archive halves from the high–magnetic susceptibility intervals (Cores 201-1225A-1H through 11H and 21H through 34H; 0–90 and 190–300 mbsf, respectively) (Shipboard Scientific Party, 2003). An automatic paleomagnetic processor NP2 (Niitsuma and Koyama, 1994) was used to measure NRM and anhysteretic remanent magnetization (ARM) in samples from Hole 1225C. NRM measurements were made with 10-mT stepwise AF demagnetization to 40 mT. ARM was measured with 10-mT steps up to 40 mT AF and a 29-µT steady direct field. The geomagnetic polarity timescale used in this study is the same as that presented by Cande and Kent (1995; CK95) (Fig. F2).

F1. Site locations, p. 10.
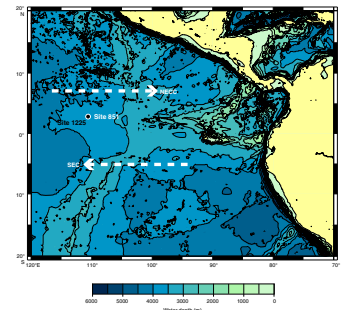
F2. Chronostratigraphy, p. 11.
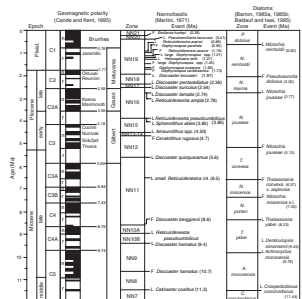
Diatom Analysis

Core catcher samples from Hole 1225A were prepared for diatom analysis using a slide preparation technique modified from Koizumi and Tanimura (1985). Each sample was dried in a 60°C oven for 24 hr. The dried sample (~50 mg) was treated with hydrogen peroxide solution (15% H_2O_2), decanted, and rinsed with deionized water. This rinsing and decanting process was repeated until the solution no longer reacted to the H_2O_2. A 1.0-mL aliquot was taken from the shaken suspension and spread evenly onto an 18-mm² coverslip. The aliquot was diluted with deionized water when the suspension was too concentrated. The coverslip was oven dried at <40°C and then mounted on a glass slide with mounting medium (refractive index = 1.78). Random field traverses of the slide were examined under the Normarskii differential interference contrast microscope at 630×. Higher magnification (1000×) was also used for taxonomic identification. Relative diatom frequencies are designated by one of the following codes (Winter and Iwai, 2002):

A = abundant (>10 valves per field of view [FOV]).
C = common (>1 valve per FOV).
F = few (>1 valve per 10 FOVs and <1 valve per FOV).
R = rare (>3 valves per transverse of coverslip and <1 valve per 10 FOVs).
+ = present (<3 valves per transverse of coverslip, including fragments).

The diatom zonation used in this study is that of Barron (1985a, 1985b) with a few modifications by Baldauf and Iwai (1995) (Fig. F2).

Nannofossil Analysis

A total of 32 samples were processed and examined using commonly accepted techniques as described by Stradner and Papp (1961). The slides were examined under an Olympus binocular polarizing microscope at a magnification of 1500× with an oil-immersion objective lens. Several thousand coccolith and *Discoaster* specimens were identified. In addition, 200 specimens were randomly counted to determine relative frequencies and stratigraphic changes of species occurrences.

Relative nannofossil frequencies are designated by one of the following codes (Takayama and Sato, 1987):

A = abundant (>32% of the species in the total assemblage).
C = common (32%–8%).
R = rare (<8%).
+ = present (found but not counted).

The calcareous nannofossil zonation used in this study is the same as that presented by Martini (1971), Takayama and Sato (1987), and Sato et al. (1999) (Fig. F2).

RESULTS

Drilling Disturbance

Coring using the ODP advanced piston corer (APC) system introduces large vertical isothermal remanent magnetization (IRM) overprints on the NRM of sediments (e.g., Acton et al., 2002). Downward and upward drilling overprints were recognized at Site 1225. Downward drilling overprints on archive-half and discrete samples were removed by <20-mT AF demagnetization (Fig. F3). Occasionally, drilling disturbance also introduces metal filings into the top of the cores. Such material was identified in Hole 1225A (Shipboard Scientific Party, 2003). This caused upward overprints that could not be removed by <20-mT AF demagnetization. Therefore, when the core catcher overlapped with the top of the next core, the uncontaminated core catcher sections were used for analysis.

Magnetostratigraphy

Polarity changes in lithologic Subunits IA (0–70 mbsf) and IC (200–255 mbsf) were observed in the declination of NRM after 15-mT AF demagnetization (Figs. F4, F5). The correlation between the observed magnetic polarities in Subunit IA of Hole 1225A and the CK95 geomagnetic polarity timescale was made carefully under the age constraints determined at Site 851 and confirmed by biostratigraphy. The Brunhes Chronozone to Cochiti Subchronozone was identified in the upper 70 mbsf (Fig. F4). The Brunhes/Matuyama (Chron C1n/Subchron C1r.1r) polarity boundary in Hole 1225A at 11.44 mbsf was in agreement with the same boundary in Holes 851B (12.75 mbsf) and 851E (11.58 mbsf). The Olduvai Subchronozone (Chron C2n) in Hole 1225A (29.2–31.36 mbsf) correlated with that in Holes 851B (28.10–30.48 mbsf) and 851C (27.80–29.85 mbsf). The magnetic directions and intensities varied in the Matuyama Chronozone (Subchrons C1r.1r–C2r.2r), so other events were unclear. The onset of the Gauss Chronozone (Subchron C2n.1n) and the termination of the Cochiti Subchronozone (Subchron C3n.1n) in Hole 1225A (60.18 and 67.36 mbsf, respectively) correlated with the same events in Hole 851B (59.72 and 67.40 mbsf), Hole 851C (59.25 and 67.95 mbsf), and Hole 851E (59.60 and 67.80 mbsf). The magnetic reversal horizons in Subunit IA of Hole 1225A were well correlated with those in Holes 851B, 851C, and 851E, although they are ~1.5 m shallower than at Site 851.

The biostratigraphic zonation, described in detail in the next section, provided age control, enabling correlation of the polarity reversals in Subunit IC (200–255 mbsf) with CK95 (Fig. F5). The last occurrence (LO) of *Discoaster hamatus* (9.4 Ma) and the LO of *Denticulopsis simonsenii* (9.45 Ma) occur between Samples 201-1225A-24H-CC and 25H-CC (224.82 and 234.30 mbsf). We defined a critical polarity boundary at 221.88 mbsf, above 224.82 mbsf, as the onset of Chron C4Ar (9.308 Ma). This definition then allows correlation of other magnetic events with CK95: terminations of Chron C4An (8.699 Ma) at 203.36 mbsf, Subchron C4Ar.2n (9.580–9.642 Ma) between 226.88 and 228.74 mbsf, and Subchron C5n.1n (9.740 Ma) at 230.06 mbsf. Figures F4 and F5 show the magnetostratigraphic interpretation for Hole 1225A.

Subunits IB and ID did not contain a magnetic reversal record and the magnetic intensity dropped to ~1×10^{-4} A/m (Fig. F3). Pyrite was a

F3. Demagnetization, p. 12.
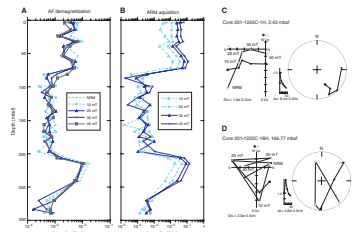
F4. Paleomagnetic measurements, 0–90 mbsf, p. 13.
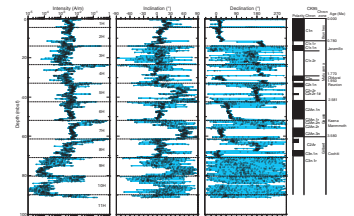
F5. Paleomagnetic measurements, 190–320 mbsf, p. 14.
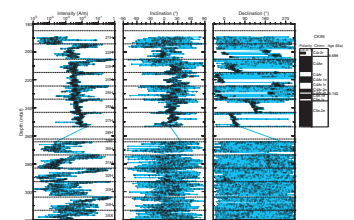
common feature of these subunits, as recorded by the lithologic descriptions (Shipboard Scientific Party, 2003). Samples from these intervals had not acquired any ARM (Fig. F3), which suggests an absence of magnetic iron sulfide minerals (pyrrhotite or greigite). X-ray diffraction analyses confirmed the visual identification of pyrite in Cores 201-1225C-22H (199.01 mbsf), 27H (251.43 mbsf), and 201-1225A-33H (294.48 mbsf) (Shipboard Scientific Party, 2003).

Biostratigraphy (Hole 1225A)

Diatoms

Diatom datums and their depths in Hole 1225A are listed in Table T1. Diatoms are present in the Quaternary (*Fragilariopsis doliolus* Zone) through upper middle Miocene (*Craspedodiscus coscinodiscus* Zone) sediments recovered from Hole 1225A. Although the LO of *Nitzschia reinholdii* is commonly used to identify the boundary between the *F. doliolus* and *N. reinholdii* Zones, it is not well constrained at this site because of the scattered occurrence of this species. Therefore, the LO of *Fragilariopsis fossilis* was used. Samples 201-1225A-1H-CC and 2H-CC were assigned to the *F. doliolus* Zone based on the occurrence of *F. doliolus* stratigraphically above the LO of *F. fossilis*. The first occurrence (FO) of *F. doliolus*, the *F. doliolus*/*Nitzschia marina* zonal boundary, was placed between Samples 201-1225A-4H-CC and 5H-CC, allowing Samples 3H-CC and 4H-CC to be assigned to the *N. reinholdii* Zone. The co-occurrence of *Rhizosolenia praebergonii* and *Thalassiosira convexa* without *Nitzschia jouseae* in Sample 201-1225A-5H-CC allowed us to assign this sample to Subzone A of the *N. marina* Zone. The presence of *N. jouseae* in Samples 201-1225A-6H-CC through 10H-CC placed these samples in the *N. jouseae* Zone. Stratigraphic floral events observed in this interval included the FO of *R. praebergonii*, placed between Samples 201-1225A-6H-CC and 7H-CC, the FO of *T. convexa* var. *convexa* between Samples 7H-CC and 8H-CC, and the LO of *Nitzschia cylindrica* between Samples 9H-CC and 10H-CC, all within the *N. jouseae* Zone.

The FO of *T. convexa* var. *aspinosa* in Sample 201-1225A-15H-CC defined the base of the *T. convexa* Zone. The FO of *Nitzschia miocenica* was placed in Sample 18H-CC, allowing placement of the interval from Sample 16-CC to 18H-CC in the *N. miocenica* Zone. Samples 16H-CC and 17H-CC contain *Thalassiosira praeconvexa* without *T. convexa*, suggesting placement of these samples in Subzone B of the *N. miocenica* Zone.

The presence of *Nitzschia porteri* without *N. miocenica* and the *Thalassiosira yabei* group in Samples 201-1225A-19H-CC through 21H-CC suggests that these samples correspond to the *N. porteri* Zone. The presence of *T. yabei* in Samples 22H-CC through 24H-CC allowed placement of these samples in the *T. yabei* Zone. The last continuous occurrence (LCO) of *Denticulopsis simonsenii* s.l. and the LO of *Actinocyclus moronensis* between Samples 24H-CC and 25H-CC allowed placement of the boundary between the *T. yabei* and *A. moronensis* Zones in this interval. The sediments from Hole 1225A have a continuous diatom biostratigraphy with a minimal age of ~11.5 Ma at the basaltic basement, the same age as Site 851. The age model based on diatoms compares favorably with the magnetic record (Fig. F6).

T1. Diatom events, p. 18.

F6. Diatom biostratigraphy, p. 15.
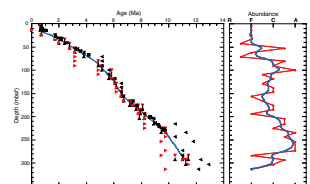
Nannofossils

Nannofossil datums and their depths in Hole 1225A are listed in Table T2. Sample 201-1225A-1H-CC was assigned to the upper Pleistocene–Holocene *Emiliania huxleyi* Zone (NN21). *E. huxleyi*, *Calcidiscus leptoporus*, *Helicosphaera carteri*, *Reticulofenestra* spp. (small), and gephyrocapsids were dominant. *Rhabdosphaera clavigera*, *Syracosphaera pulchra*, and *Umbilicosphaera sibogae* were frequent. The presence of *Pseudoemiliania lacunosa* in Samples 2H-CC to 7H-CC indicates an early Pleistocene–late Pliocene age (Zones NN19–NN16) for these samples. Sample 2H-CC included *Reticulofenestra asanoi,* which indicates calcareous nannofossil Datum 7 in the Quaternary (Sato et al., 1999).

The Pliocene/Pleistocene boundary was placed between Samples 201-1225A-3H-CC and 4H-CC. Sample 7H-CC was assigned to Zone NN18 (*Discoaster brouweri* Zone). *D. brouweri*, *Discoaster pentaradiatus*, and *Discoaster surculus* were present in Sample 5H-CC, which was placed in Zone NN16 (*D. surculus* Zone). Below this sample, discoasters gradually increased in number of species. *Discoaster tamalis* was found below Sample 6H-CC. Sample 8H-CC contained *Reticulofenestra pseudoumbilicus* together with *Sphenolithus abies*. The occurrence of *Amaurolithus* spp. and *Ceratolithus rugosus* in Samples 10H-CC and 11H-CC indicates the lower Pliocene (Zones NN13~NN14). The presence of *Discoaster quinqueramus* places Sample 14H-CC within the upper Miocene *D. quinqueramus* Zone (Subzone NN11B). Samples 18H-CC to 22H-CC were characterized by small coccolith and *Discoaster* assemblages. *R. pseudoumbilicus* was once again present below Sample 23H-CC. Samples 25H-CC and 26H-CC may belong to Zone NN9 (*D. hamatus* Zone) on the basis of the occurrence of *D. hamatus*. The occurrence of *Discoaster kugleri* in Samples 33H-CC and 34H-CC indicates the middle Miocene (Zones NN7~NN8).

The age model based on nannofossils compares favorably with the magnetic record (Fig. F7).

DISCUSSION

The age model based on magnetostratigraphy and biostratigraphy in Hole 1225A is very consistent (Fig. F8). In Subunit IA (0–70 mbsf), polarity reversals are consistent with diatom and nannofossil datums through the last 4.2 m.y., yielding a sedimentation rate of 1.7 cm/k.y.

In the low–magnetic intensity interval (70–200 mbsf), diatom zonation was useful for age determination between 5 and 9 Ma, with a sedimentation rate of 3.3 cm/k.y. Within Subunit IC, from 200 to 230 mbsf, polarity reversals are well correlated with diatoms and nannofossils from 8.6 to 9.7 Ma, with a sedimentation rate of 2.7 cm/k.y. In Subunit ID (255–300 mbsf), a low–magnetic intensity unit, diatom and nannofossil events coincide within a range of 1 to 2 m.y. The sedimentation rate is ~3.6 cm/k.y., based on diatom zonation.

Subunits IB and ID have higher sedimentation rates and correspond to the late Miocene–early Pliocene biogenic bloom event (4.5–7 Ma) and the Miocene global cooling trend (10–15 Ma) (Farrell et al., 1995; Cortese et al., 2004). The higher sedimentation rates and prevalence of pyrite in these subunits suggest that high biogenic productivity led to the pyritization of magnetic minerals and the destruction of the magnetic signal. There is also evidence that basement fluid is penetrating Subunit ID (Oyun et al., 1995; Shipboard Scientific Party, 2003), which could result in the dissolution of iron minerals.

T2. Zonation summary, p. 19.

F7. Nannofossil biostratigraphy, p. 16.
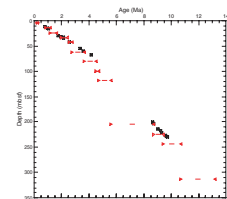
F8. Combined age-depth plot, p. 17.
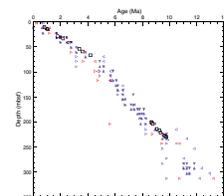
CONCLUSIONS

The magnetostratigraphy from Subunits IA and IC (0–70 and 200–255 mbsf, respectively) in Hole 1225A correlates well with diatom and nannofossil biostratigraphy. Subunit IA contains magnetic reversals until the termination of the Cochiti Subchronozone (Subchron C3n.1n; 3.8 Ma). Subunit IC was constrained by the LOs of *D. hamatus* (9.4 Ma) and *D. simonsenii* (9.45 Ma) and contains magnetic reversals between Chrons C4n.2r and C5n.2n (8.6 and 9.7 Ma). The consistency of the biostratigraphy and magnetostratigraphy indicates that reversals are adequately preserved for the age model.

Subunits IB and ID (70–200 and 255–300 mbsf, respectively) were dominated by pyrite and had no reversal record. These subunits correspond to higher sedimentation rates, which suggests that high biogenic productivity in relation to global climatic events led to the destruction of the magnetic signal. In Subunit ID, basement flow is another factor that may be altering the magnetic signal.

ACKNOWLEDGMENTS

REFERENCES

Acton, G.D., Okada, M., Clement, B.M., Lund, S.P., and Williams, T., 2002. Paleomagnetic overprints in ocean sediment cores and their relationship to shear deformation caused by piston coring. *J. Geophys. Res.,* 107. doi:10.1029/2001JB000518

Baldauf, J.G., and Iwai, M., 1995. Neogene diatom biostratigraphy for the eastern equatorial Pacific Ocean, Leg 138. *In* Pisias, N.G., Mayer, L.A., Janecek, T.R., Palmer-Julson, A., and van Andel, T.H. (Eds.), *Proc. ODP, Sci. Results,* 138: College Station, TX (Ocean Drilling Program), 105–128.

Barron, J.A., 1985a. Late Eocene to Holocene diatom biostratigraphy of the equatorial Pacific Ocean, Deep Sea Drilling Project Leg 85. *In* Mayer, L., Theyer, F., Thomas, E., et al., *Init. Repts. DSDP,* 85: Washington (U.S. Govt. Printing Office), 413–456.

Barron, J.A., 1985b. Miocene to Holocene planktic diatoms. *In* Bolli, H.M., Saunders, J.B., and Perch-Nielsen, K. (Eds.), *Plankton Stratigraphy:* Cambridge (Cambridge Univ. Press), 763–809.

Cande, S.C., and Kent, D.V., 1995. Revised calibration of the geomagnetic polarity timescale for the Late Cretaceous and Cenozoic. *J. Geophys. Res.,* 100:6093–6095. doi:10.1029/94JB03098

Cortese, G., Gersonde, R., Hillenbrand, C.-D., and Kuhn, G., 2004. Opal sedimentation shifts in the World Ocean over the last 15 Myr. *Earth Planet. Sci. Lett.*, 224:509–527. doi:10.1016/j.epsl.2004.05.035

Farrell, J.W., Raffi, I., Janecek, T.C., Murray, D.W., Levitan, M., Dadey, K.A., Emeis, K.-C., Lyle, M., Flores, J.-A., and Hovan, S., 1995. Late Neogene sedimentation patterns in the eastern equatorial Pacific Ocean. *In* Pisias, N.G., Mayer, L.A., Janecek, T.R., Palmer-Julson, A., and van Andel, T.H. (Eds.), *Proc. ODP, Sci. Results,* 138: College Station, TX (Ocean Drilling Program), 717–756.

Koizumi, I., and Tanimura, Y., 1985. Neogene diatom biostratigraphy of the middle latitude western north Pacific, Deep Sea Drilling Project Leg 86. *In* Heath, G.R., Burckle, L.H., et al., *Init. Repts. DSDP,* 86: Washington (U.S. Govt. Printing Office), 269–300.

Martini, E., 1971. Standard Tertiary and Quaternary calcareous nannoplankton zonation. *In* Farinacci, A. (Ed.), *Proc. 2nd Int. Conf. Planktonic Microfossils Roma:* Rome (Ed. Tecnosci.), 2:739–785

Niitsuma, N., and Koyama, M., 1994. Paleomagnetic processor: a fully automatic portable spinner magnetometer combined with an AF demagnetizer and magnetic susceptibility anisotropy meter. *Shizuoka Univ. Geosci. Rep.,* 21:11–19.

Oyun, S., Elderfield, H., and Klinkhammer, G.P., 1995. Strontium isotopes in pore waters of east equatorial Pacific sediments: indicators of seawater advection through oceanic crust and sediments. *In* Pisias, N.G., Mayer, L.A., Janecek, T.R., Palmer-Julson, A., and van Andel, T.H. (Eds.), *Proc. ODP, Sci. Results,* 138: College Station, TX (Ocean Drilling Program), 813–819.

Pisias, N.G., Mayer, L.A., Janecek, T.R., Palmer-Julson, A., and van Andel, T.H. (Eds.), 1995. *Proc. ODP, Sci Results,* 138: College Station, TX (Ocean Drilling Program).

Sato, T., Kameo, K., and Mita, I., 1999. Validity of the latest Cenozoic calcareous nannofossil datums and its application to the tephrochronology. *Earth Sci.,* 53:265–274.

Shipboard Scientific Party, 1992. Site 851. *In* Mayer, L., Pisias, N., Janecek, T., et al., *Proc. ODP, Init. Repts.,* 138 (Pt. 2): College Station, TX (Ocean Drilling Program), 891–965.

Shipboard Scientific Party, 2003. Site 1225. *In* D'Hondt, S.L., Jørgensen, B.B., Miller, D.J., et al., *Proc. ODP, Init. Repts.,* 201, 1–86 [CD-ROM]. Available from: Ocean Drilling Program, Texas A&M University, College Station TX 77845-9547, USA. [HTML]

Stradner, H., and Papp, A., 1961. Tertiäre Discoasteriden aus Österreich und deren stratigraphischen Bedeutung mit Hinweisen auf Mexico, Rumänien und Italien. *Jahrb. Geol. Bundesanst. (Austria),* 7:1–159.

Takayama, T., and Sato, T., 1987. Coccolith biostratigraphy of the North Atlantic Ocean, Deep Sea Drilling Project Leg 94. *In* Ruddiman, W.F., Kidd, R.B., Thomas, E., et al., *Init. Repts. DSDP,* 94 (Pt. 2): Washington (U.S. Govt. Printing Office), 651–702.

Winter, D., and Iwai, M., 2002. Data report: Neogene diatom biostratigraphy, Antarctic Peninsula Pacific margin, ODP Leg 178 rise sites. *In* Barker, P.F., Camerlenghi, A., Acton, G.D., and Ramsay, A.T.S. (Eds.), *Proc. ODP, Sci. Results,* 178 [Online]. Available from World Wide Web: <**http://www-odp.tamu.edu/publications/ 178_SR/chap_29/chap_29.htm**> [Cited 2005-01-03].

Figure F1. Location of ODP Leg 201 Site 1225 (black circle) and Leg 138 Site 851 (white circle). Site 1225 was adjacent to Leg 138 Site 851. NECC = North Equatorial Countercurrent, SEC = South Equatorial Current.
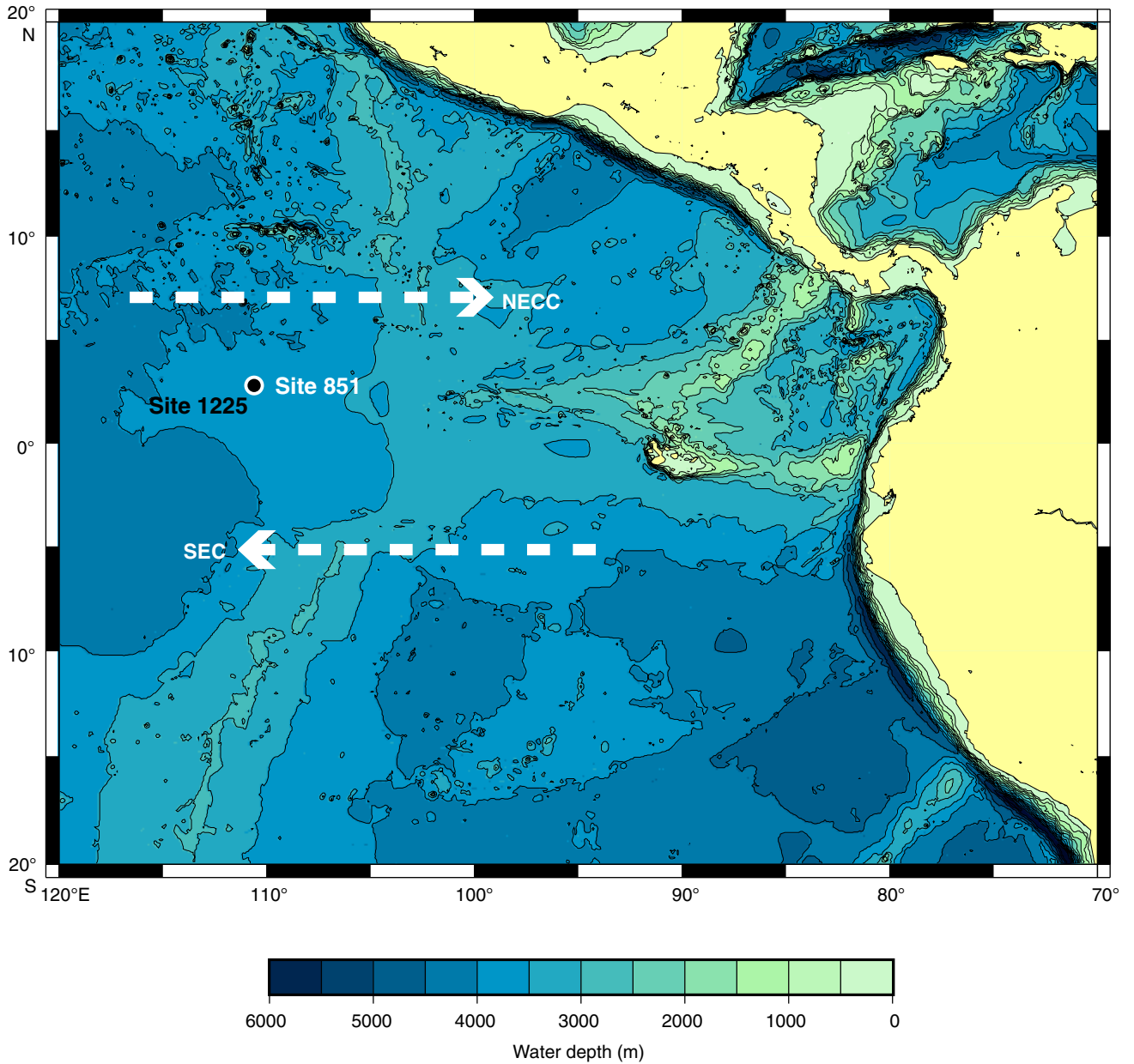
Figure F2. Summary of the Neogene chronostratigraphy adopted for Hole 1225A. F = first occurrence, L = last occurrence.
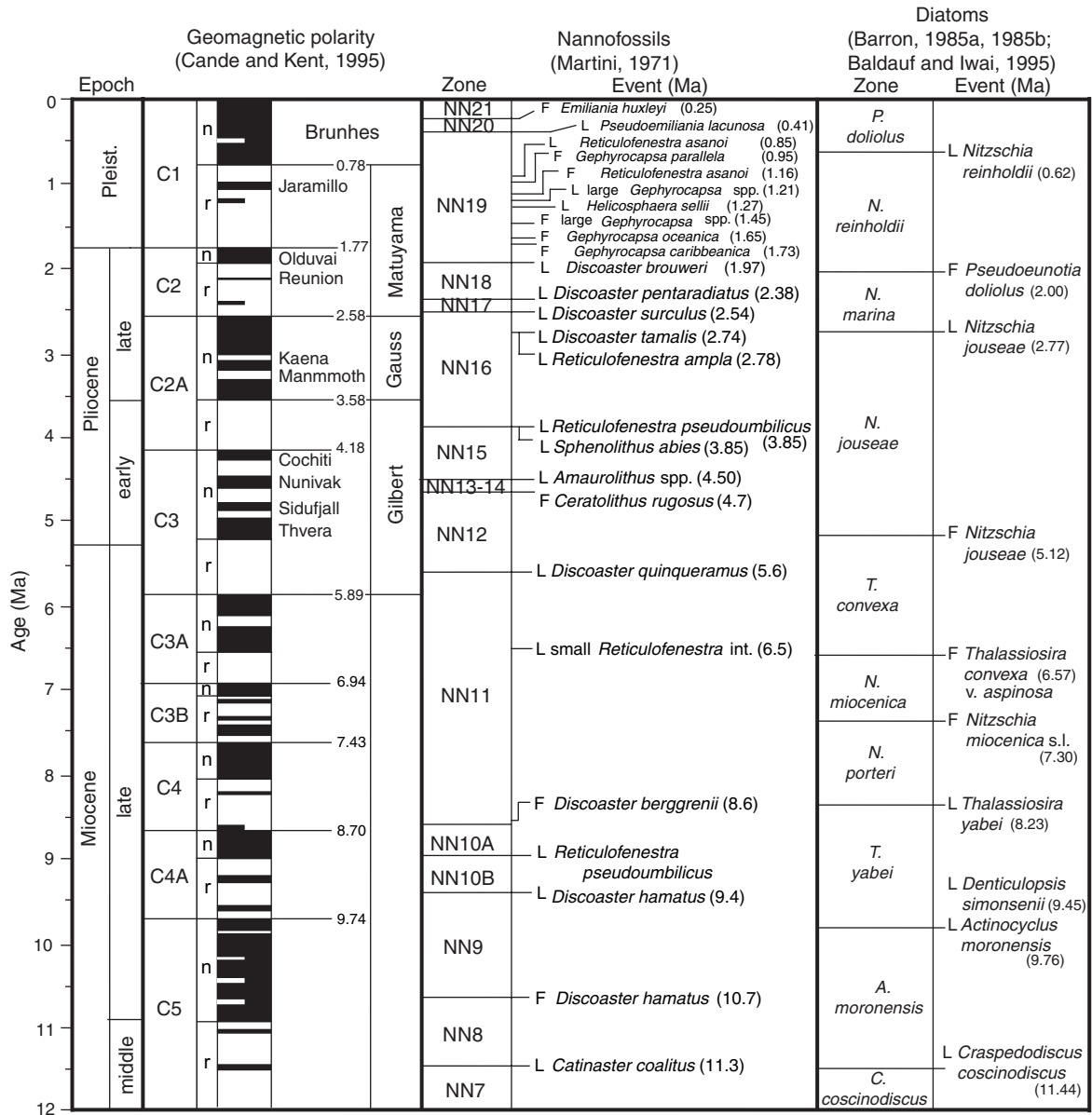
Figure F3. A. Stepwise demagnetization of natural remanent magnetization (NRM). **B.** Stepwise acquisition of anhysteretic remanent magnetization (ARM) for 29 discrete samples from Hole 1225C. **C.** Demagnetization plot of typical sample from Subunit IB that showed downward drilling overprint. **D.** Demagnetization plot of typical sample from Subunit IB that did not show magnetic direction.
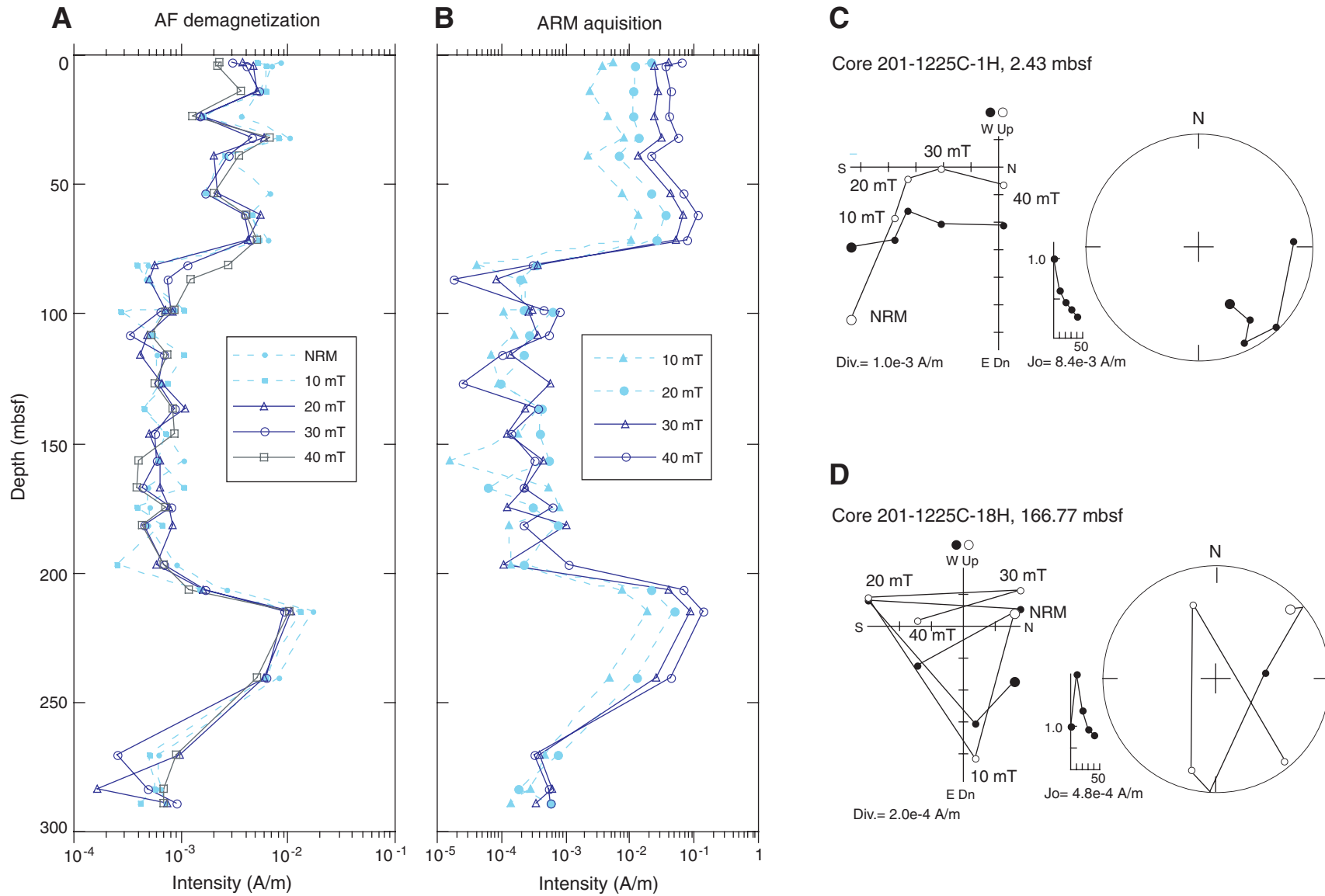
Figure F4. Magnetic intensity, declination, and inclination of NRM after AF demagnetization (15 mT) with magnetostratigraphic interpretation for Hole 1225A at 0–90 mbsf. CK95 = Cande and Kent (1995) geomagnetic polarity timescale.
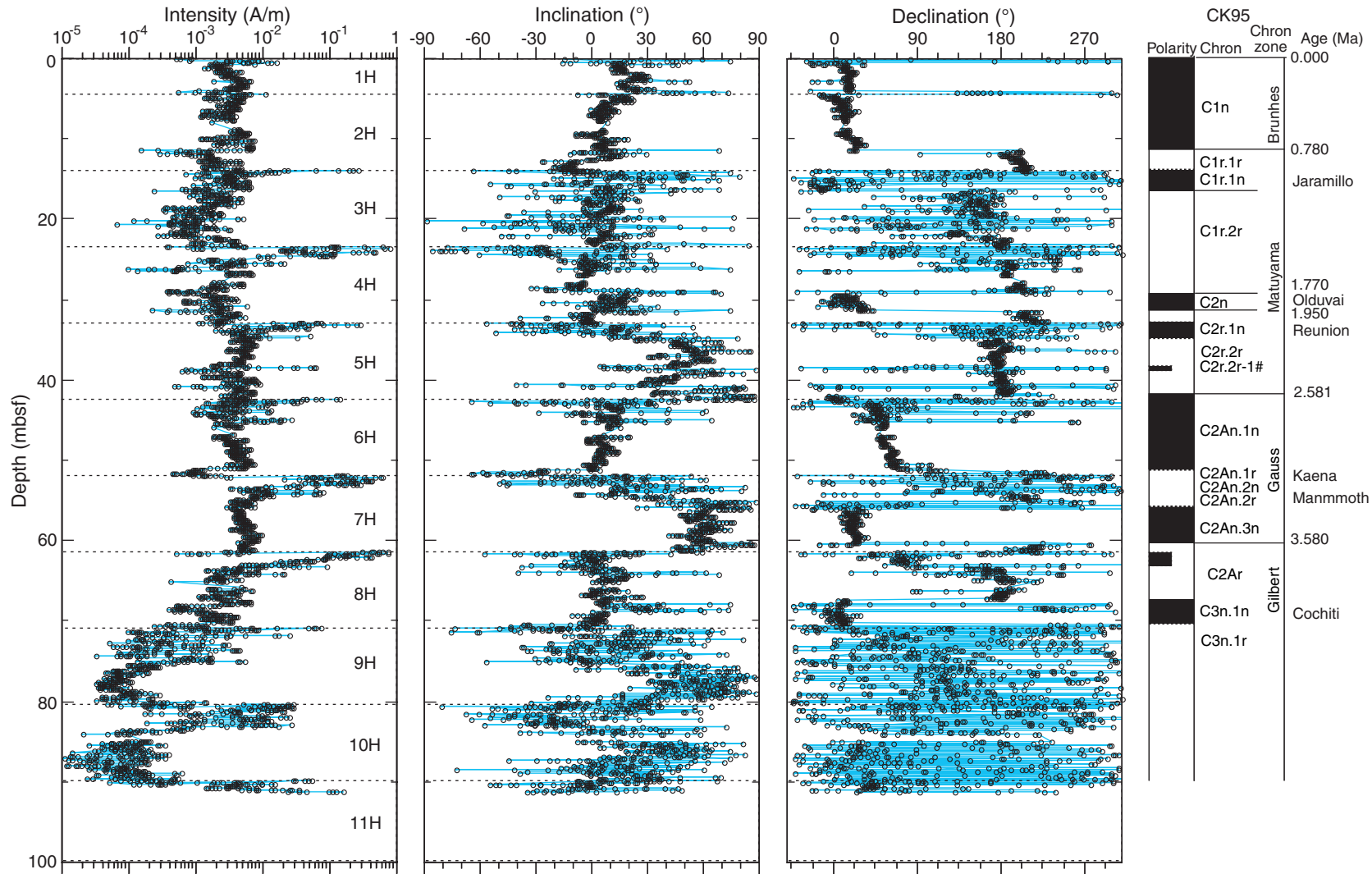
Figure F5. Magnetic intensity, declination, and inclination of NRM after AF demagnetization (15 mT) with magnetostratigraphic interpretation for Hole 1225A at 190–320 mbsf. CK95 = Cande and Kent (1995) geomagnetic polarity timescale.
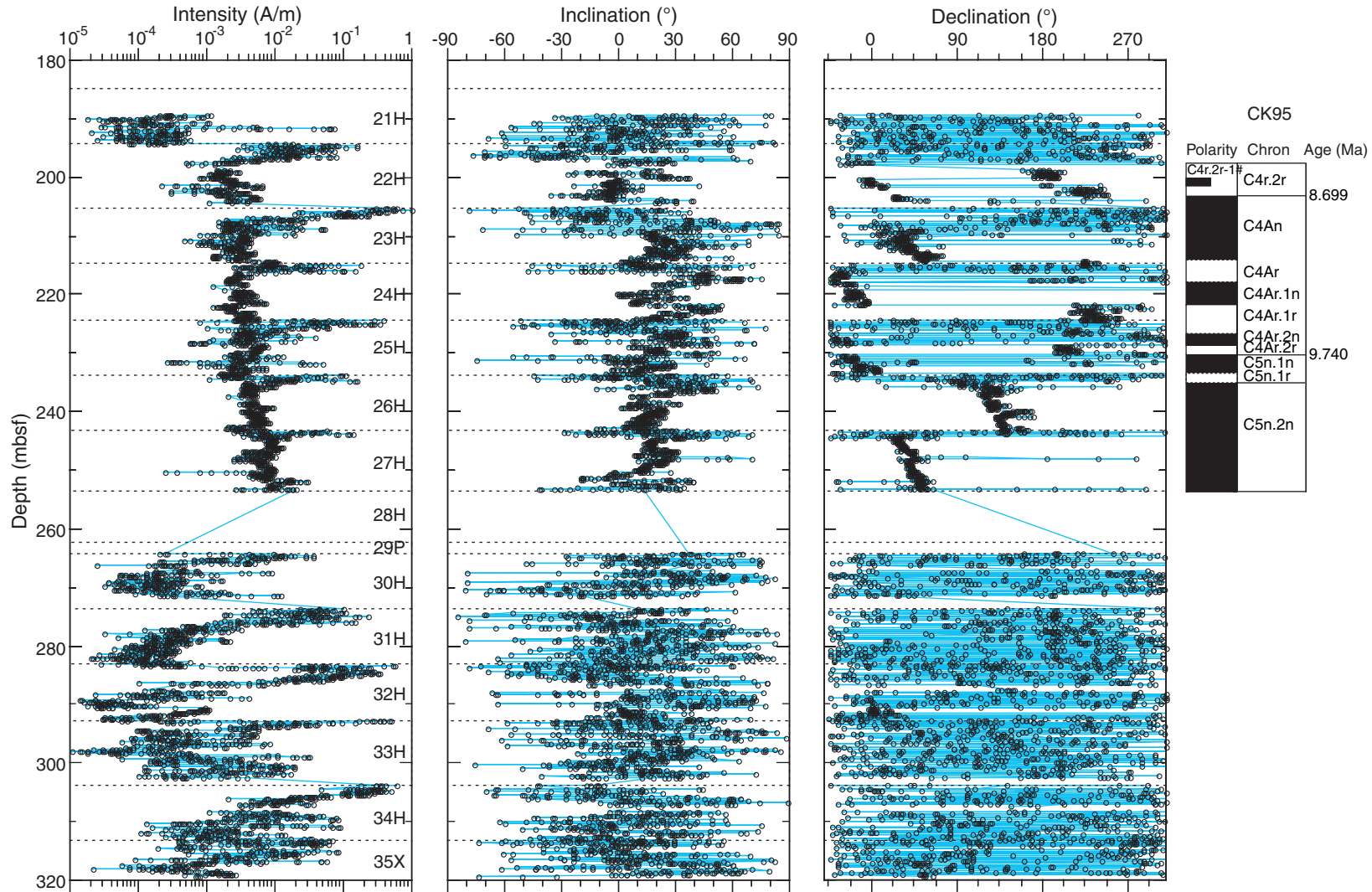
Figure F6. Age-depth plot based on diatom biostratigraphy in Hole 1225A. Solid black and red triangles show bottom and top of each diatom event. Open black and red triangles show oldest and youngest ages of each samples. Open squares show paleomagnetic stratigraphy points. A = abundant, C = common, F = few, and R= rare.
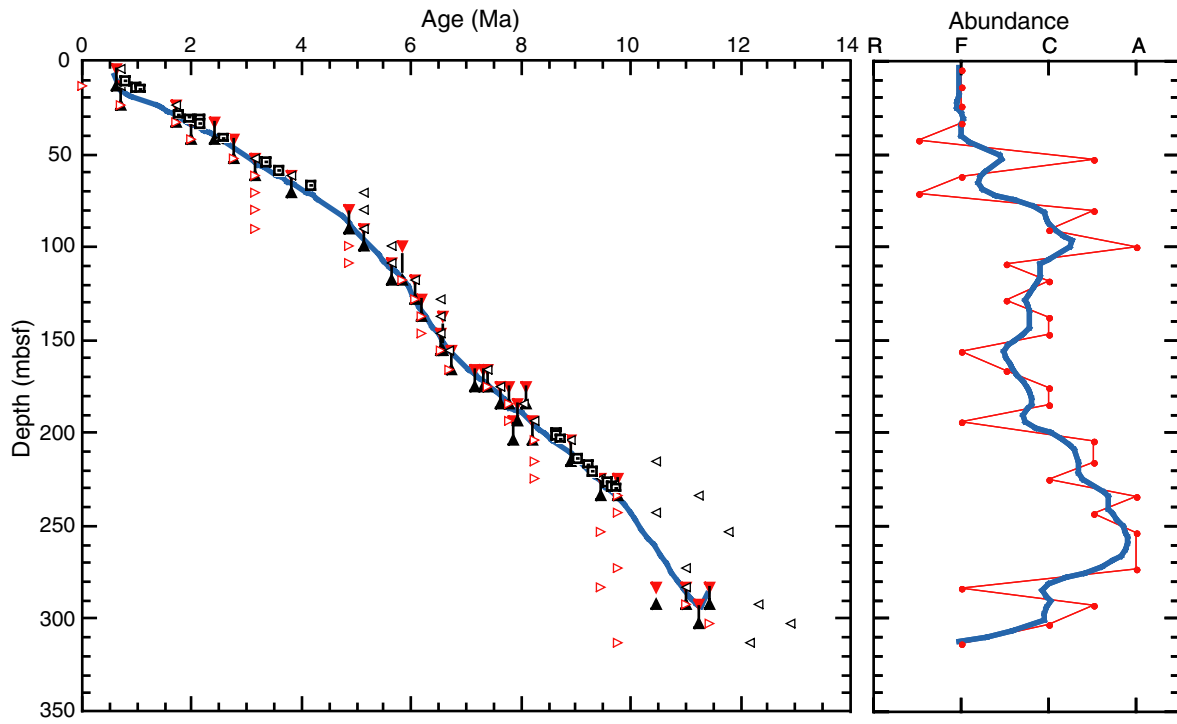
Figure F7. Age-depth plot based on nannofossil biostratigraphy (red triangles) and magnetostratigraphy (open squares) in Hole 1225A.
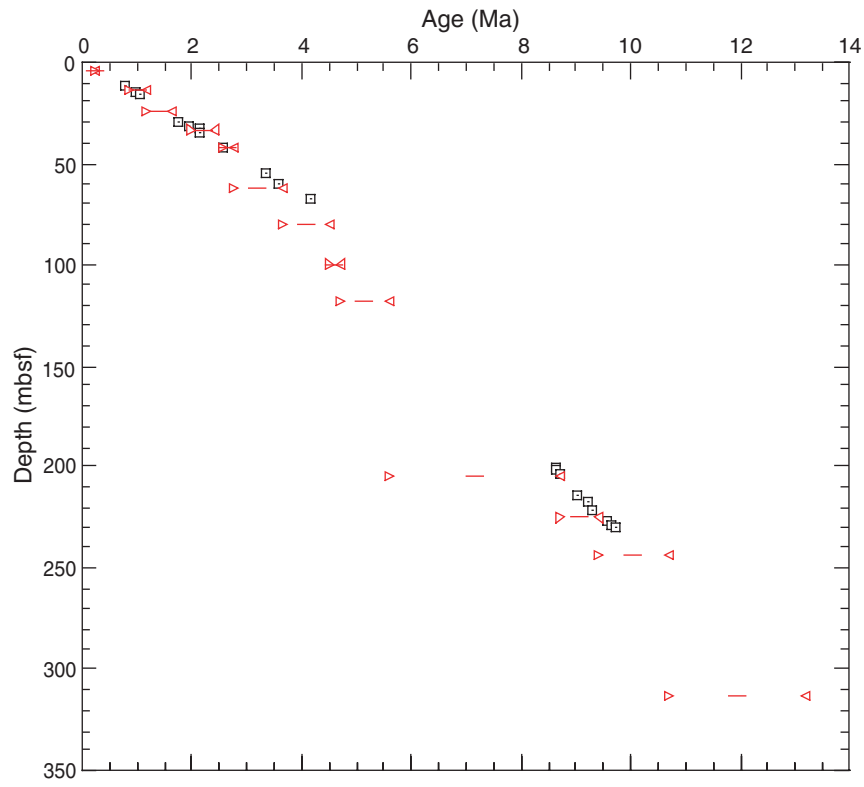
Figure F8. Age-depth plot based on magnetostratigraphy (black squares) diatom (blue triangles) and nannofossil (red triangles) biostratigraphy at Hole 1225A. Solid triangles show bottom and top of each diatom event. Open triangles show oldest and youngest ages of diatoms and nannofossils for each sample.
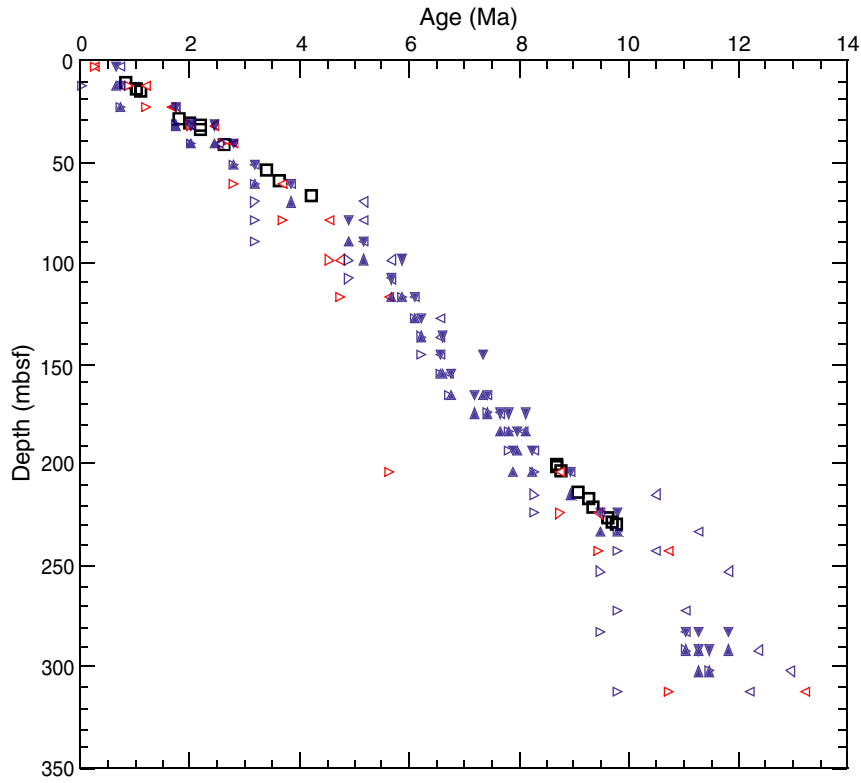
Table T1. Stratigraphically useful diatom events, Hole 1225A.

Core, section (top/bottom)	Depth (mbsf)	Event	Age* (Ma)
201-1225A-			
1H-CC/2H-CC	4.26–14.30	**LO** *Nitzschia reinholdii*	**0.62**
2H-CC/3H-CC	14.30–23.62	LO *Nitzschia fossilis*	0.70
		LO *Rhizosolenia matuyamai*	1.05
		FO *Rhizosolenia matuyamai*	1.18
3H-CC/4H-CC	23.62–33.08	LO *Rhizosolenia praebergonii* var. *robusta*	1.73
4H-CC/5H-CC	33.08–42.93	**FO** *Pseudoeunotia doliolus*	**2.00**
		LO *Thalassiosira convexa* s.l.	2.41
5H-CC/6H-CC	42.93–52.38	**LO** *Nitzschia jouseae*	**2.77**
6H-CC/7H-CC	52.38–61.72	FO *Rhizosolenia praebergonii* s.l.	3.17
7H-CC/8H-CC	61.72–71.28	FO *Thalassiosira convexa* var. *convexa*	3.81
		FO *Asteromphalus elegans*	3.99
9H-CC/10H-CC	80.79–90.34	LO *Nitzschia cylindrica*	4.88
10H-CC/11HCC	90.34–99.79	**FO** *Nitzschia jouseae*	**5.12**
12H-CC/13H-CC	109.23–118.81	FO *Thalassiosira oestrupii*	5.64
11H-CC/13H-CC	99.79–118.81	LO *Thalassiosira miocenica*	5.84
13H-CC/14H-CC	118.81–128.50	LO *Nitzschia miocenica* s.s.	6.08
		LO *Nitzschia miocenica* var. *elongata*	6.08
14H-CC/15H-CC	128.50–137.75	LO *Thalassiosira praeconvexa*	6.18
16H-CC/17H-CC	147.50–156.33	LO *Rossiella praepaleacea*	6.54
		FO *Thalassiosira miocenica*	6.55
15H-CC/17H-CC	137.75–156.33	**FO** *Thalassiosira convexa* **var.** *aspinosa*	**6.57**
17H-CC/18H-CC	156.33–166.05	FO *Thalassiosira praeconvexa*	6.71
18H-CC/19H-CC	166.05–175.75	LO *Nitzschia porteri*	7.16
		FO *Nitzschia miocenica* **s.l.**	**7.30**
		LO *Rossiella paleacea*	7.40
19H-CC/20H-CC	175.75–185.23	FO *Nitzschia reinholdii*	7.64
		LO *Actinocyclus ellipticus* var. *javanicus*	7.79
21H-CC/22H-CC	194.39–204.23	LO *Thalassiosira burckliana*	7.85
20H-CC/21H-CC	185.23–194.39	FO *Nitzschia marina*	7.95
19H-CC/20H-CC	175.75–185.23	FO *Nitzschia cylindrica*	8.07
21H-CC/22H-CC	194.39–204.23	**LO** *Thalassiosira yabei*	**8.23**
		LO *Coscinodiscus loeblichii*	8.86
22H-CC/23H-CC	204.23–215.38	FO *Thalassiosira burckliana*	8.91
24H-CC/25H-CC	224.82–234.30	**LO** *Denticulopsis simonsenii*	**9.45**
		FO *Coscinodiscus loeblichii*	9.65
24H-CC/25H-CC	224.82–234.30	**LO** *Actinocyclus moronensis*	**9.76**
31H-CC/32H-CC	283.79–293.17	FO *Actinocyclus ellipticus* f. *lanceolata*	10.45
		LO *Denticulopsis*	11.02
		LO *Coscinodiscus gigas* var. *diorama*	11.23
32H-CC/33H-CC	293.17–302.70	FO *Rossiella paleacea* var. *elongata*	11.23
31H-CC/32H-CC	283.79–293.17	**LO** *Craspedodiscus coscinodiscus*	**11.44**
—	—	LO *Synedra jouseana*	11.51
—	—	FO *Hemidiscus cuneiformis*	11.80
—	—	**LCO** *Actinocyclus ingens* **s.s.**	**12.18**
—	—	LO *Cestodiscus pulchellus*	12.23
—	—	FO *Thalassiosira brunii*	12.28
—	—	FO *Nitzschia porteri*	12.32
—	—	LO *Crucidenticula*	12.47
—	—	LO *Annellus californicus*	12.53

Notes: Datums occur in the cores within the interval listed for each species. * = Cande and Kent (1995). LO = last occurrence datum, FO = first occurrence datum, FCO = first common occurrence datum, LCO = last common occurrence datum. Events in bold designate boundaries of each diatom zone. — = interval drilled but not cored or not drilled.

Table T2. Summary of Neogene nannofossils, Hole 1225A.

Core, section	Depth (mbsf)	Epoch	Age (Ma)	Zone	Amaurolithus spp.	Calcidiscus leptoporus	Calcidiscus macintyrei	Catinaster coalitus	Ceratolithus spp.	Coccolithus pelagicus	Coccolithus miopelagicus	Cyclithella annulus	Discoaster asymmetricus	Discoaster bellus	Discoaster brouweri	Discoaster calcaris	Discoaster challengeri	Discoaster exilis	Discoaster hamatus	Discoaster kugleri	Discoaster loeblichii	Discoaster pentaradiatus	Discoaster quadramus	Discoaster quinqueramus	Discoaster surculus	Discoaster tamalis	Discoaster triradiatus	Discoaster variabilis	Discoaster spp.	Discolithina japonica	Discolithina multipora	Discolithina spp.	Emiliania huxleyi	Gephyrocapsa carribeanica	Gephyrocapsa oceanica	Gephyrocapsa parallela	Gephyrocapsa spp. (small)	Helicosphaera carteri	Helicosphaera granulata	Helicosphaera hyalina	Helicosphaera intermedia	Helicosphaera sellii	Helicosphaera wallichii	Pseudoemiliania lacunosa	Reticulofenestra asanoi	Reticulofenestra pseudoumbilicus	Reticulofenestra spp. (small)	Rhabdosphaera clavigera	Sphenolithus abies	Sphenolithus moriformis	Syracosphaera pulchra	Umbilicosphaera sibogae
201-1225A-																																																			
1H-CC	3.94	Pleistocene	~0.25	NN21		C																											C	C	C	C	A	C		R							C	R			R	R	
2H-CC	14.10		0.85~1.16	NN19		C	+		+	+																								A		A	A					C	C		R	+	A				R	R	
3H-CC	23.39		1.16~1.65			C																									+			R	A	A	R				C	C				A				R	R	
4H-CC	32.85		2.00~2.40	NN18		R	R		+	C					R											R					+	+	R			R	C			C		+	R	R				A				+	+
5H-CC	42.59	Pliocene (late)	2.56~2.75	NN16		C	R		R	C					R							R			R			R		R				R			C				R	+	R	R				A					+
6H-CC	52.14		2.75~3.66	NN16		C	+		R	C		R	+		R							R			R	R		R	R	C			C			+	C				R		R	R				A			R		
7H-CC	61.31			NN16		C	R		R	R			+	+	C										+	+	R	C			C							R			R		+					A				+	+
8H-CC	71.06		3.66~4.50	NN15		R	R		+				R		R										+	R	R				R							C									A	A	C		+	+
9H-CC	80.39			NN15		R			R			+		R	C							+			R		C	A	+		R							C					+				C	A	C		+	R
10H-CC	90.09	Pliocene (early)	4.50~4.70	NN13~14	+	C	+		+	+	R		R		C							+			C	+	C	A	+		R							C									C	A	A			
11H-CC	99.54			NN13~14	R	C			+	C			R		C							R			C		+	C	A	+		R						R						+				C	A	C			+
12H-CC	108.97		4.70~5.60	NN12	+	C	+						+		R							+			R		R	A	R	R	R							R					R					C	A	C			
13H-CC	118.56			NN12	R	C									R							+			R		R	A	R	R								C					+				C	A	A			
14H-CC	128.09	Miocene (late)		NN11B	R	C				R					R							R	R		R		R	A	R	R								C					R				C	A	A			
15H-CC	137.48					C				C	+				R			+				C		R	R		R	A	R	R								R								R	A	A	+		
16H-CC	147.20					C				C	R				R							+	+	R	R			C	R								+									C	A	C			
17H-CC	156.16		5.60~8.70	NN10B~11A		C	R			C					R			+				+	+	C	C			R										C					+				R	A	A			
18H-CC	165.80					C	R			C					C						+	R			R	R	C	A								R				R					A	C			
19H-CC	175.47					C				C					R					R			+	+	R	R	R	A								C									A	C			
20H-CC	184.94					C	R			C					R	R	R			R	R			R	C			+						R	C					+					A	A	R		
21H-CC	194.39					C				C					R	R	R			R	R		R	R	C										C				+					A	A	R		
22H-CC	203.96					R	R			C		R			R	+	R			+	C		R		A										C		+		+	+				C	A	R		
23H-CC	215.13		8.70~9.40	NN10A		+				R	R				R		C							C																				C	A	C	C		
24H-CC	224.62					R	+			R	R				R			+						R									+		C				+				C	A	C	R		
25H-CC	234.03		9.40~10.70	NN9		R	+			C	+		+				+	R	+	R				C							+			+		C								C	A	C	R		
26H-CC	243.53					C		R		C		R			R	R	R		+					C								R		C								C	C	C			
27H-CC	252.98					R	+			C					+		R							+	C								R		R								C	R	C	R		
30H-CC	272.81	Miocene (middle)		NN7~8		+				C	R				+									R	C		+							R		R								A	C	R	R		
31H-CC	283.43		10.70~13.20			R				C	R				+		R							R	C								R		R								C	A		R		
32H-CC	292.88					R				C	R					R	R								C								R		R	+				+				C	A				
33H-CC	302.40					R				R	R				+	+			R					+	C					R			R		R	+				+				C	A		R	R	
34H-CC	313.48					C	+			C	C				+	+			+						A						R		R		C	R				+				A	A		R	R	

Notes: Biostratigraphic zonation from Martini (1971), bioevents datum from Sato et. al. (1999), and diatom biostratigraphic zonation from Barron (1985a, 1985b) and Baldauf and Iwai (1995). Relative frequencies (Takayama and Sato, 1987): A = abundant (>32% of the species in total assemblage), C = common (32%–8%), R = rare (<8%), + = present (found but not counted).